Neural Enhancement of Analytical Appearance Models: Supplemental Material

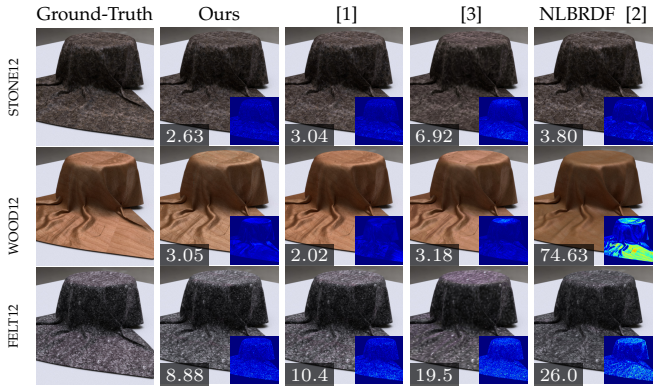

Fig. 1: Comparisons with NLBRDF [2] and neural BTF models [1] and [3] on 3 BTFs from UBO [4] dataset. From the first column to last, ground-truths, results of our enhanced GGX, neural BTF models [1], [3], and NLBRDF [2], respectively. Quantitative error, computed as the mean squared error ($\times 10^4$), is reported at the bottom-left of each related image, and the error map is shown at the bottom-right.

1 BTFs

While our primary focus is on measured BRDFs, we demonstrate that our approach is also applicable to certain measured BTFs. In Fig. 1, we compare with state-of-the-art methods [1], [2], [3] on BTFs from the UBO dataset [4]. Our results are more accurate than NLBRDF [2] and [3], because we explicitly model the local frame and anisotropic reflections. In addition, our quality is comparable to a dedicated BTF model [1]. Moreover, our footprint for each BTF texel is 39 floats, comparable to 32 in their approach, but our network size is about 1/5 of theirs.

Despite this success, we also show a failure case in Fig. 2. Our model cannot fit the fabric12 BTF from the UBO dataset with high quality, as it considerably deviates from our training data. In the future, we plan to include more diverse training data to improve the final quality on such samples.

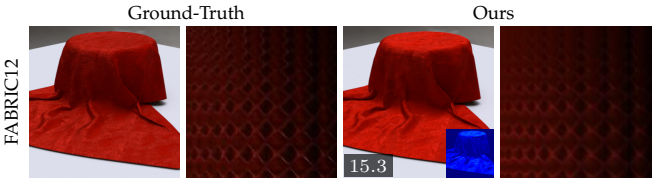

Fig. 2: Limitation. From the first column to last, rendered result of ground-truth, visualization of one ground-truth BTF pixel (horizontal axis: light, vertical axis: view), rendered result of our model, and visualization of a corresponding BTF pixel from our model.

2 Additional BRDF Results

Finally, Fig. 3 visualizes the neural enhancement results across the entire set of materials from the EPFL dataset [5], comparing our enhanced versions of GGX, Cook-Torrance, Ward, and GenBRDF models against their original counterparts, as well as NBRDF and NLBRDF. In Fig. 4, we perform similar comparisons on the materials from the UTIA dataset [6]. For methodology details and further analysis, please refer to the main paper.

Fig. 3: Neural enhancement of several analytical BRDF models on materials from EPFL dataset [5]. From the first column to last, the ground-truths, the results of enhanced/original Cook-Torrance BRDF model with GGX distribution, enhanced/original Cook-Torrance model, enhanced/original Ward model, enhanced/original FULL model in GenBRDF, NBRDF [11], and NLBRDF [2]. Quantitative errors in SSIM and ΔE_{ITP} ($\times 10^3$) are reported in the bottom-left of each related image.

Fig. 3: (*Continued.*) Neural enhancement of several analytical BRDF models on materials from EPFL dataset [5]. From the first column to last, the ground-truths, the results of enhanced/original Cook-Torrance BRDF model with GGX distribution, enhanced/original Cook-Torrance model, enhanced/original Ward model, enhanced/original FULL model in GenBRDF, NBRDF [11], and NLBRDF [2]. Quantitative errors in SSIM and ΔE_{ITP} ($\times 10^3$) are reported in the bottom-left of each related image.

Fig. 3: (*Continued.*) Neural enhancement of several analytical BRDF models on materials from EPFL dataset [5]. From the first column to last, the ground-truths, the results of enhanced/original Cook-Torrance BRDF model with GGX distribution, enhanced/original Cook-Torrance model, enhanced/original Ward model, enhanced/original FULL model in GenBRDF, NBRDF [11], and NLBRDF [2]. Quantitative errors in SSIM and ΔE_{ITP} ($\times 10^3$) are reported in the bottom-left of each related image.

Fig. 3: (*Continued.*) Neural enhancement of several analytical BRDF models on materials from EPFL dataset [5]. From the first column to last, the ground-truths, the results of enhanced/original Cook-Torrance BRDF model with GGX distribution, enhanced/original Cook-Torrance model, enhanced/original Ward model, enhanced/original FULL model in GenBRDF, NBRDF [11], and NLBRDF [2]. Quantitative errors in SSIM and ΔE_{ITP} ($\times 10^3$) are reported in the bottom-left of each related image.

Fig. 3: (*Continued.*) Neural enhancement of several analytical BRDF models on materials from EPFL dataset [5]. From the first column to last, the ground-truths, the results of enhanced/original Cook-Torrance BRDF model with GGX distribution, enhanced/original Cook-Torrance model, enhanced/original Ward model, enhanced/original FULL model in GenBRDF, NBRDF [11], and NLBRDF [2]. Quantitative errors in SSIM and ΔE_{ITP} ($\times 10^3$) are reported in the bottom-left of each related image.

Fig. 3: (*Continued.*) Neural enhancement of several analytical BRDF models on materials from EPFL dataset [5]. From the first column to last, the ground-truths, the results of enhanced/original Cook-Torrance BRDF model with GGX distribution, enhanced/original Cook-Torrance model, enhanced/original Ward model, enhanced/original FULL model in GenBRDF, NBRDF [11], and NLBRDF [2]. Quantitative errors in SSIM and ΔE_{ITP} ($\times 10^3$) are reported in the bottom-left of each related image.

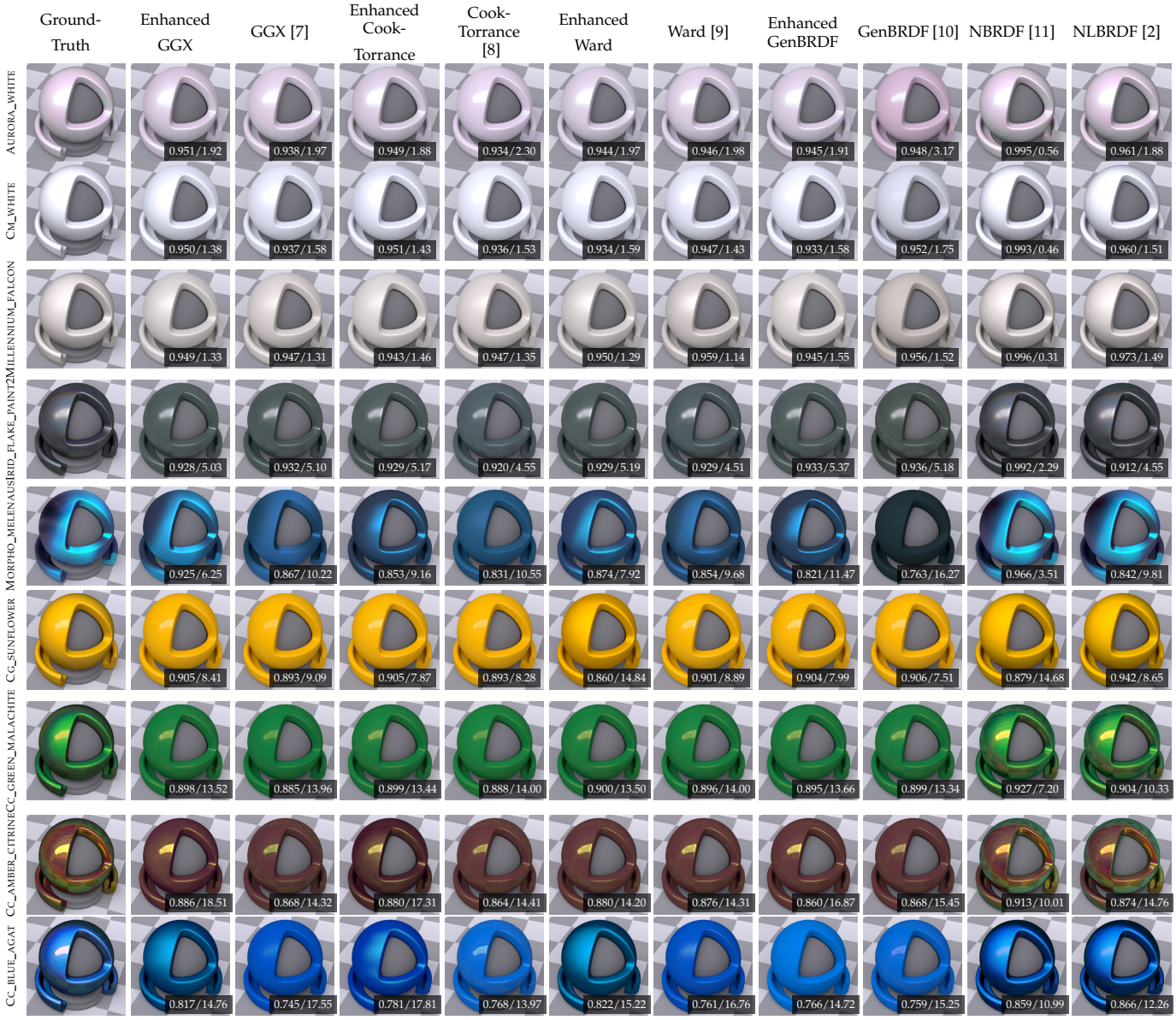

Fig. 3: (*Continued.*) Neural enhancement of several analytical BRDF models on materials from EPFL dataset [5]. From the first column to last, the ground-truths, the results of enhanced/original Cook-Torrance BRDF model with GGX distribution, enhanced/original Cook-Torrance model, enhanced/original Ward model, enhanced/original FULL model in GenBRDF, NBRDF [11], and NLBRDF [2]. Quantitative errors in SSIM and ΔE_{ITP} ($\times 10^3$) are reported in the bottom-left of each related image.

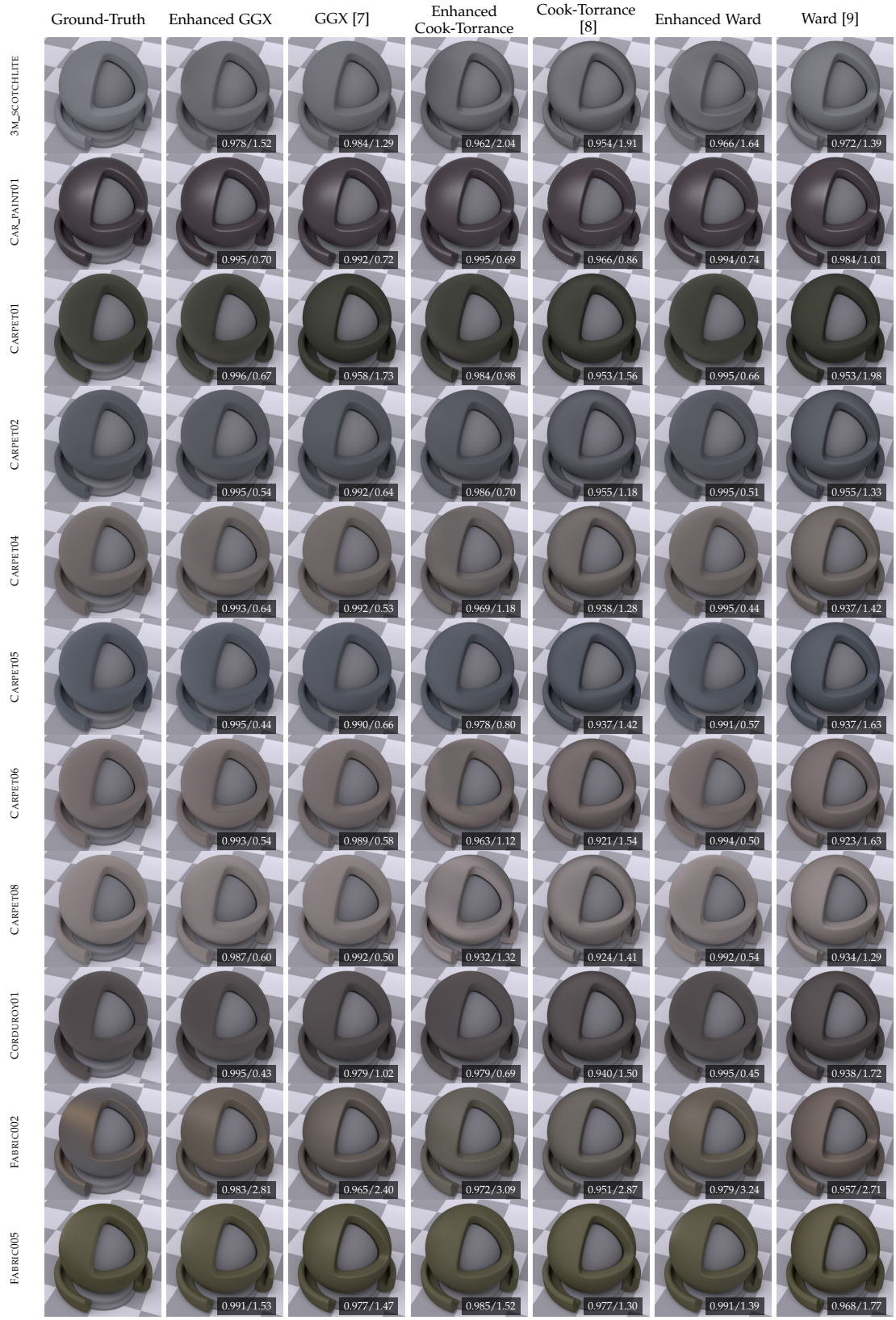

Fig. 4: Neural enhancement of several analytical BRDF models on materials from UTIA dataset [6]. From the first column to last, the ground-truths, the results of enhanced/original Cook-Torrance BRDF model with GGX distribution, enhanced/original Cook-Torrance model, and enhanced/original Ward model. Quantitative errors in SSIM and ΔE_{ITP} ($\times 10^3$) are reported in the bottom-left of each related image.

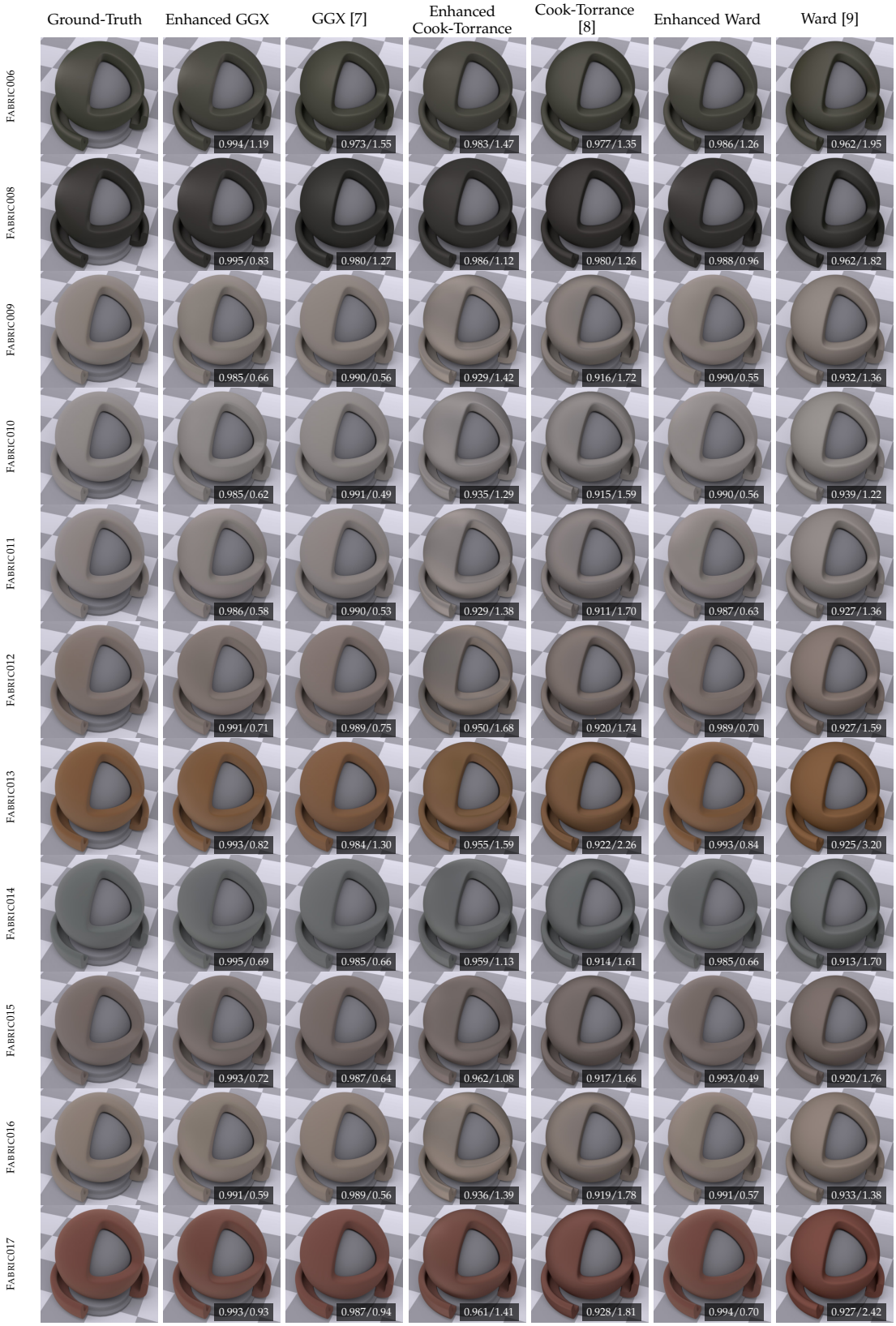

Fig. 4: (*Continued.*) Neural enhancement of several analytical BRDF models on materials from UTIA dataset [6]. From the first column to last, the ground-truths, the results of enhanced/original Cook-Torrance BRDF model with GGX distribution, enhanced/original Cook-Torrance model, and enhanced/original Ward model. Quantitative errors in SSIM and ΔE_{ITP} ($\times 10^3$) are reported in the bottom-left of each related image.

Fig. 4: (*Continued.*) Neural enhancement of several analytical BRDF models on materials from UTIA dataset [6]. From the first column to last, the ground-truths, the results of enhanced/original Cook-Torrance BRDF model with GGX distribution, enhanced/original Cook-Torrance model, and enhanced/original Ward model. Quantitative errors in SSIM and ΔE_{ITP} ($\times 10^3$) are reported in the bottom-left of each related image.

Fig. 4: (*Continued.*) Neural enhancement of several analytical BRDF models on materials from UTIA dataset [6]. From the first column to last, the ground-truths, the results of enhanced/original Cook-Torrance BRDF model with GGX distribution, enhanced/original Cook-Torrance model, and enhanced/original Ward model. Quantitative errors in SSIM and ΔE_{ITP} ($\times 10^3$) are reported in the bottom-left of each related image.

Fig. 4: (*Continued.*) Neural enhancement of several analytical BRDF models on materials from UTIA dataset [6]. From the first column to last, the ground-truths, the results of enhanced/original Cook-Torrance BRDF model with GGX distribution, enhanced/original Cook-Torrance model, and enhanced/original Ward model. Quantitative errors in SSIM and ΔE_{ITP} ($\times 10^3$) are reported in the bottom-left of each related image.

Fig. 4: (*Continued.*) Neural enhancement of several analytical BRDF models on materials from UTIA dataset [6]. From the first column to last, the ground-truths, the results of enhanced/original Cook-Torrance BRDF model with GGX distribution, enhanced/original Cook-Torrance model, and enhanced/original Ward model. Quantitative errors in SSIM and ΔE_{ITP} ($\times 10^3$) are reported in the bottom-left of each related image.

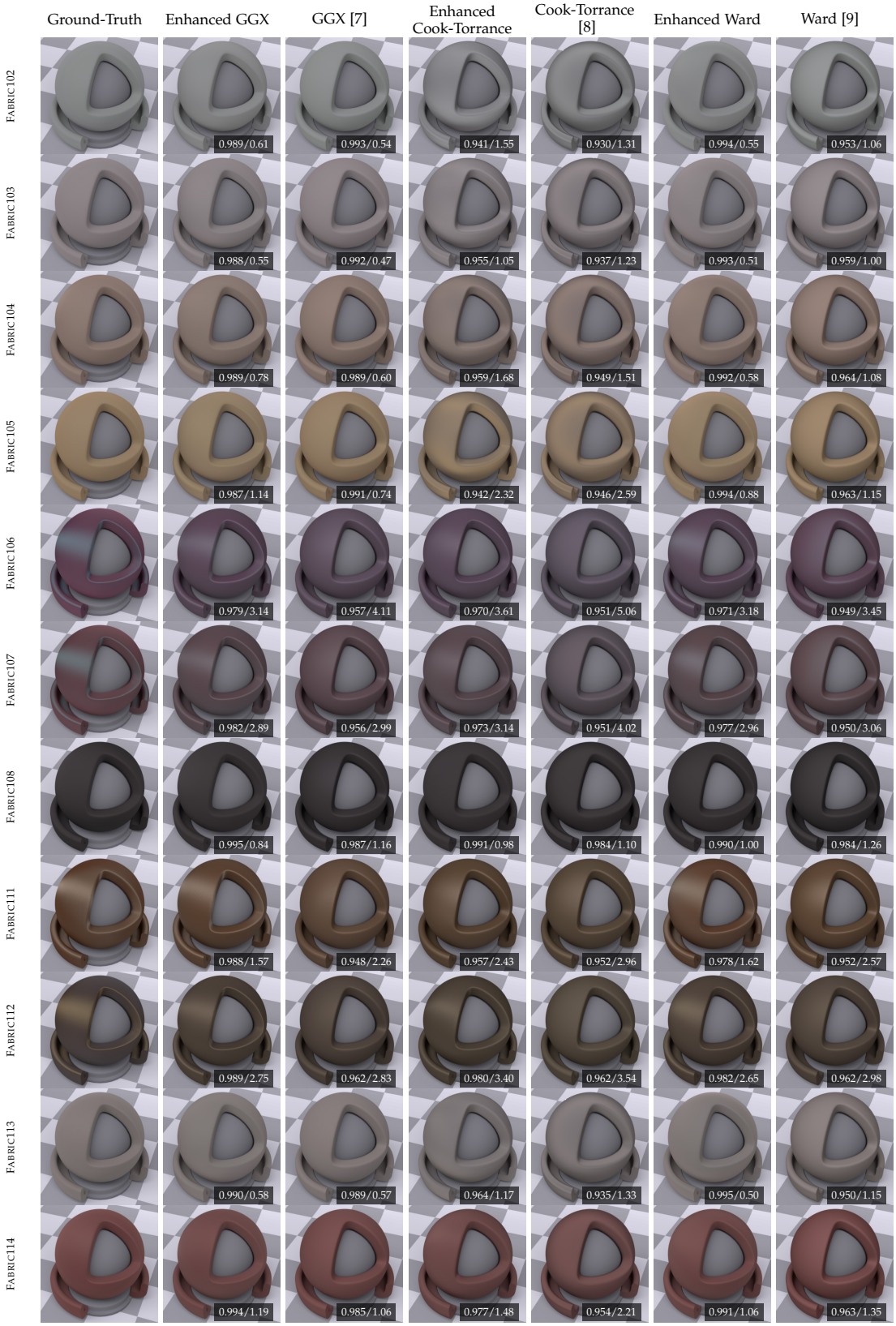

Fig. 4: (*Continued.*) Neural enhancement of several analytical BRDF models on materials from UTIA dataset [6]. From the first column to last, the ground-truths, the results of enhanced/original Cook-Torrance BRDF model with GGX distribution, enhanced/original Cook-Torrance model, and enhanced/original Ward model. Quantitative errors in SSIM and ΔE_{ITP} ($\times 10^3$) are reported in the bottom-left of each related image.

Fig. 4: (*Continued.*) Neural enhancement of several analytical BRDF models on materials from UTIA dataset [6]. From the first column to last, the ground-truths, the results of enhanced/original Cook-Torrance BRDF model with GGX distribution, enhanced/original Cook-Torrance model, and enhanced/original Ward model. Quantitative errors in SSIM and ΔE_{ITP} ($\times 10^3$) are reported in the bottom-left of each related image.

Fig. 4: (*Continued.*) Neural enhancement of several analytical BRDF models on materials from UTIA dataset [6]. From the first column to last, the ground-truths, the results of enhanced/original Cook-Torrance BRDF model with GGX distribution, enhanced/original Cook-Torrance model, and enhanced/original Ward model. Quantitative errors in SSIM and ΔE_{ITP} ($\times 10^3$) are reported in the bottom-left of each related image.

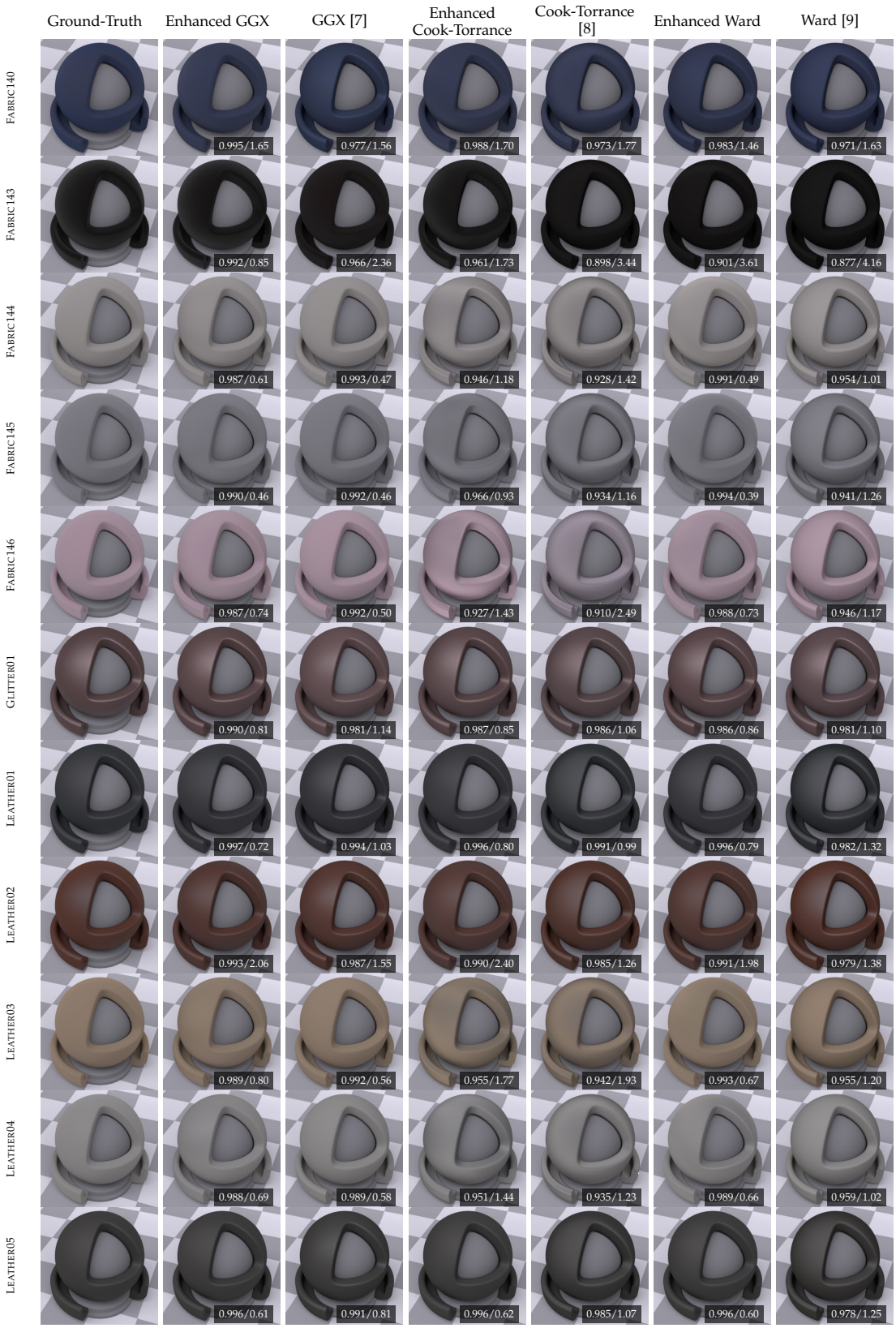

Fig. 4: (*Continued.*) Neural enhancement of several analytical BRDF models on materials from UTIA dataset [6]. From the first column to last, the ground-truths, the results of enhanced/original Cook-Torrance BRDF model with GGX distribution, enhanced/original Cook-Torrance model, and enhanced/original Ward model. Quantitative errors in SSIM and ΔE_{ITP} ($\times 10^3$) are reported in the bottom-left of each related image.

Fig. 4: (*Continued.*) Neural enhancement of several analytical BRDF models on materials from UTIA dataset [6]. From the first column to last, the ground-truths, the results of enhanced/original Cook-Torrance BRDF model with GGX distribution, enhanced/original Cook-Torrance model, and enhanced/original Ward model. Quantitative errors in SSIM and ΔE_{ITP} ($\times 10^3$) are reported in the bottom-left of each related image.

Fig. 4: (*Continued.*) Neural enhancement of several analytical BRDF models on materials from UTIA dataset [6]. From the first column to last, the ground-truths, the results of enhanced/original Cook-Torrance BRDF model with GGX distribution, enhanced/original Cook-Torrance model, and enhanced/original Ward model. Quantitative errors in SSIM and ΔE_{ITP} ($\times 10^3$) are reported in the bottom-left of each related image.

Fig. 4: (*Continued.*) Neural enhancement of several analytical BRDF models on materials from UTIA dataset [6]. From the first column to last, the ground-truths, the results of enhanced/original Cook-Torrance BRDF model with GGX distribution, enhanced/original Cook-Torrance model, and enhanced/original Ward model. Quantitative errors in SSIM and ΔE_{ITP} ($\times 10^3$) are reported in the bottom-left of each related image.

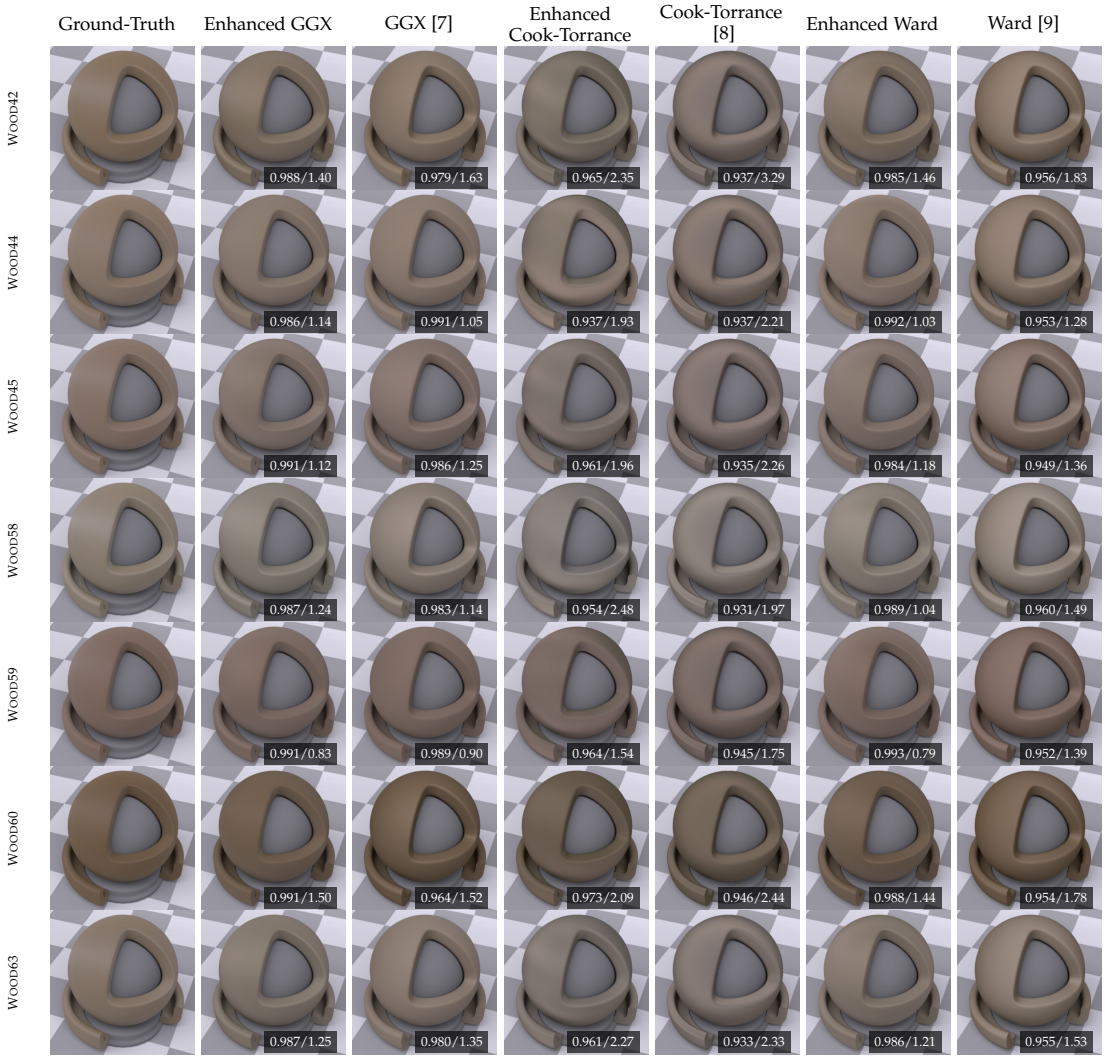

Fig. 4: (*Continued.*) Neural enhancement of several analytical BRDF models on materials from UTIA dataset [6]. From the first column to last, the ground-truths, the results of enhanced/original Cook-Torrance BRDF model with GGX distribution, enhanced/original Cook-Torrance model, and enhanced/original Ward model. Quantitative errors in SSIM and ΔE_{ITP} ($\times 10^3$) are reported in the bottom-left of each related image.

REFERENCES

[1] G. Rainer, A. Ghosh, W. Jakob, and T. Weyrich, "Unified neural encoding of btfs," in Computer Graphics Forum, vol. 39, pp. 167–178, Wiley Online Library, 2020.

[2] J. Fan, B. Wang, M. Hasan, J. Yang, and L.-Q. Yan, "Neural layered brdfs," in ACM SIGGRAPH 2022 Conference Proceedings, SIGGRAPH '22, (New York, NY, USA), Association for Computing Machinery, 2022.

[3] B. Xue, S. Zhao, H. W. Jensen, and Z. Montazeri, "A hierarchical architecture for neural materials," Computer Graphics Forum, vol. 43, no. 6, p. e15116, 2024.

[4] M. Weinmann, J. Gall, and R. Klein, "Material classification based on training data synthesized using a btf database," in Computer Vision–ECCV 2014: 13th European Conference, Zurich, Switzerland, September 6-12, 2014, Proceedings, Part III 13, pp. 156–171, Springer, 2014.

[5] J. Dupuy and W. Jakob, "An adaptive parameterization for efficient material acquisition and rendering," ACM Transactions on graphics (TOG), vol. 37, no. 6, pp. 1–14, 2018.

[6] J. Filip and R. Vávra, "Template-based sampling of anisotropic brdfs," in Computer Graphics Forum, vol. 33, pp. 91–99, Wiley Online Library, 2014.

[7] B. Walter, S. R. Marschner, H. Li, and K. E. Torrance, "Microfacet models for refraction through rough surfaces," in Proceedings of the 18th Eurographics conference on Rendering Techniques, pp. 195–206, 2007.

[8] R. L. Cook and K. E. Torrance, "A reflectance model for computer graphics," ACM Transactions on Graphics (ToG), vol. 1, no. 1, pp. 7–24, 1982.

[9] G. J. Ward, "Measuring and modeling anisotropic reflection," in Proceedings of the 19th annual conference on Computer graphics and interactive techniques, pp. 265–272, 1992.

[10] A. Brady, J. Lawrence, P. Peers, and W. Weimer, "genbrdf: Discovering new analytic brdfs with genetic programming," ACM Transactions on Graphics (TOG), vol. 33, no. 4, pp. 1–11, 2014.

[11] A. Sztrajman, G. Rainer, T. Ritschel, and T. Weyrich, "Neural brdf representation and importance sampling," in Computer Graphics Forum, vol. 40, pp. 332–346, Wiley Online Library, 2021.